ACS chemical biology

Articles

pubs.acs.org/acschemicalbiology

Design of Protease Activated Optical Contrast Agents That Exploit a Latent Lysosomotropic Effect for Use in Fluorescence-Guided Surgery

Leslie O. Ofori,[†] Nimali P. Withana,[†] Tyler R. Prestwood,[‡] Martijn Verdoes,[†,¶] Jennifer J. Brady,[∥] Monte M. Winslow,[†,∥] Jonathan Sorger,[⊥] and Matthew Bogyo*[,†,§]

Departments of [†]Pathology, [‡]Medicine, [§]Microbiology & Immunology, and [∥]Genetics, Stanford University School of Medicine, 300 Pasteur Drive, Stanford, California 94035, United States

[⊥]Intuitive Surgical Inc., 1020 Kifer Road, Sunnyvale, California 94086, United States

Supporting Information

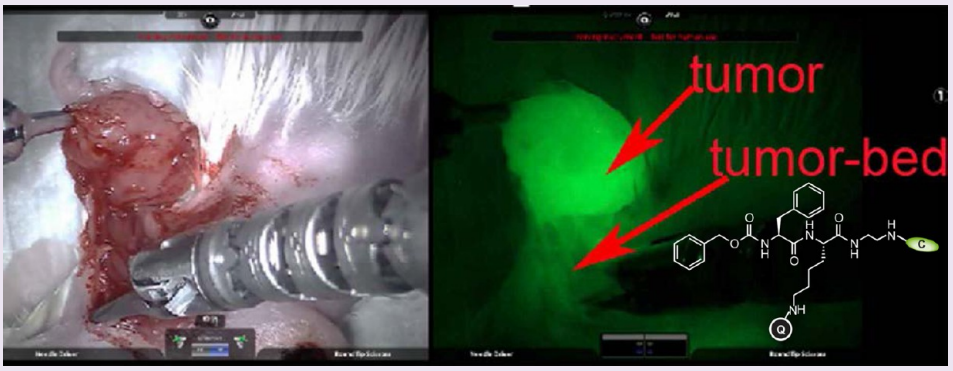

ABSTRACT: There is a need for new molecular-guided contrast agents to enhance surgical procedures such as tumor resection that require a high degree of precision. Cysteine cathepsins are highly up-regulated in a wide variety of cancers, both in tumor cells and in the tumor-supporting cells of the surrounding stroma. Therefore, tools that can be used to dynamically monitor their activity *in vivo* could be used as imaging contrast agents for intraoperative fluorescence image guided surgery (FGS). Although multiple classes of cathepsin-targeted substrate probes have been reported, most suffer from overall fast clearance from sites of protease activation, leading to reduced signal intensity and duration *in vivo*. Here we describe the design and synthesis of a series of near-infrared fluorogenic probes that exploit a latent cationic lysosomotropic effect (LLE) to promote cellular retention upon protease activation. These probes show tumor-specific retention, fast activation kinetics, and rapid systemic distribution. We demonstrate that they are suitable for detection of diverse cancer types including breast, colon and lung tumors. Most importantly, the agents are compatible with the existing, FDA approved, da Vinci surgical system for fluorescence guided tumor resection. Therefore, our data suggest that the probes reported here can be used with existing clinical instrumentation to detect tumors and potentially other types of inflammatory lesions to guide surgical decision making in real time.

INTRODUCTION

Surgical intervention is currently the most common treatment for virtually all types of solid tumors.[1,2] A successful outcome is therefore contingent upon the complete removal of all cancer cells from both the affected primary organ and from potential metastatic sites during surgery.[3] Contrast agents that target specific biomarkers in cancers can be used as intraoperative contrast agents to guide surgical resection of solid tumors in order to improve treatment outcome.[4,5] Among the diverse imaging modalities, optical-based techniques utilizing fluorescent contrast agents have great potential.[6,7] Indocyanine green (ICG), fluorescein, methylene blue, and 5-aminolevulinic acid (5-ALA) are all nontargeted contrast agents that are currently used as injectable enhancers for the visualization of various tumors.[8,9] In addition, several targeted contrast agents are in various stages of clinical development.[10] Notably, an FITC probe that targets folate receptor-α was used in a clinical trial to demonstrate the value of intraoperative FGS for the treatment of ovarian cancer.[11] Additionally, other tumor-targeting agents such as Chlorotoxin-Cy5.5 have been validated for optical imaging of malignant cancer cells using various mouse models of cancer. However, its mechanism of tumor selectivity is not well understood.[12]

An alternative approach to general tumor-targeted contrast agents is the use of so-called "smart probes" that only produce or accumulate a signal in tumor tissues when acted upon by an

Received: March 22, 2015
Accepted: June 3, 2015
Published: June 3, 2015

DOI: 10.1021/acschembio.5b00205
ACS Chem. Biol. 2015, 10, 1977−1988

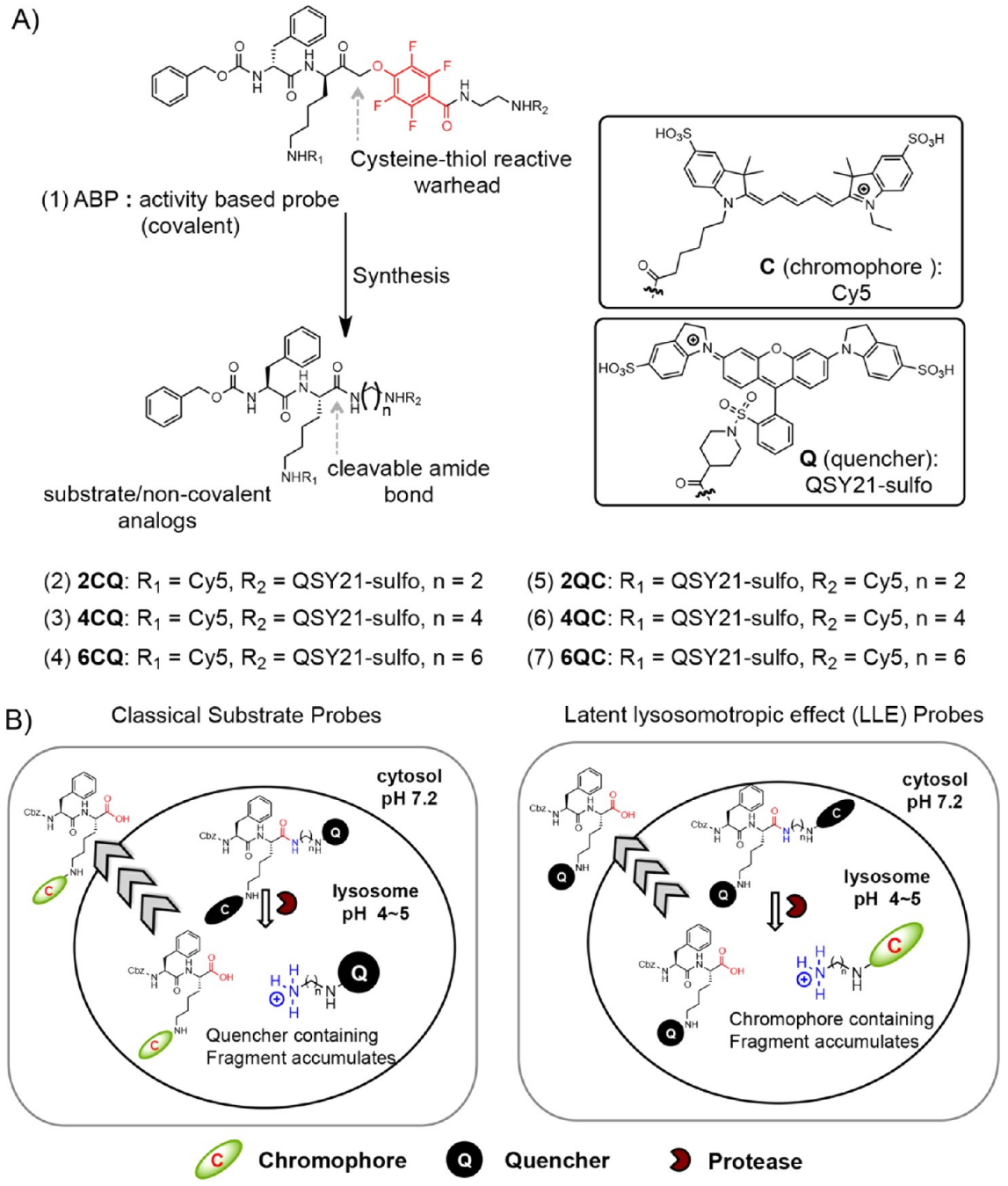

Figure 1. Design of substrate probes based on an existing quenched fluorescent activity based probe (qABP). (A) Chemical structure of a recently reported broad-spectrum cysteine cathepsin qABP (1) and the design of a set of six substrate analogues by replacement of the phenoxymethyl ketone (PMK) electrophile with a cleavable amide bond. In the *n*CQ substrates (2−4; where *n* spacer length = 2, 4, 6), the chromophore (C) is attached to the lysine side chain (R_1) and the quenching group (Q) is attached on the C-terminal side of the cleavable amide bond (R_2), whereas in the *n*QC substrates (5−7), the location of each is inverted. (B) Schematic representation of the latent lysosomotropic effect that results in improved retention of the cleaved fluorescent products of probe cleavage.

enzyme activity that is associated with the tumor or surrounding margins. A common strategy for enzyme-activated smart probe design is to engineer probes that produce signal when cleaved by a protease. Because proteases play significant roles in tumor growth and metastasis as well as in diverse pathologies such as fibrosis, inflammation, osteoporosis, arthritis, contrast agents that are activated by proteases could prove valuable for detection and treatment of many diseases.[13,14]

A number of probes for tumor imaging applications have targeted the matrix metallo proteases (MMPs) due to their reported roles in angiogenesis and tumor growth. This includes both small molecule and large polymer-based probes[15−17] that produce a signal upon cleavage as well as masked cell penetrating peptides that accumulate inside cells when cleaved by an MMP.[18,19] As an alternative to the MMPs, the cysteine cathepsins are important regulators of various aspects of tumorigenesis.[20] These proteases are also highly expressed and activated in many cells that regulate the intrinsic inflammatory

DOI: 10.1021/acschembio.5b00205
ACS Chem. Biol. 2015, 10, 1977−1988

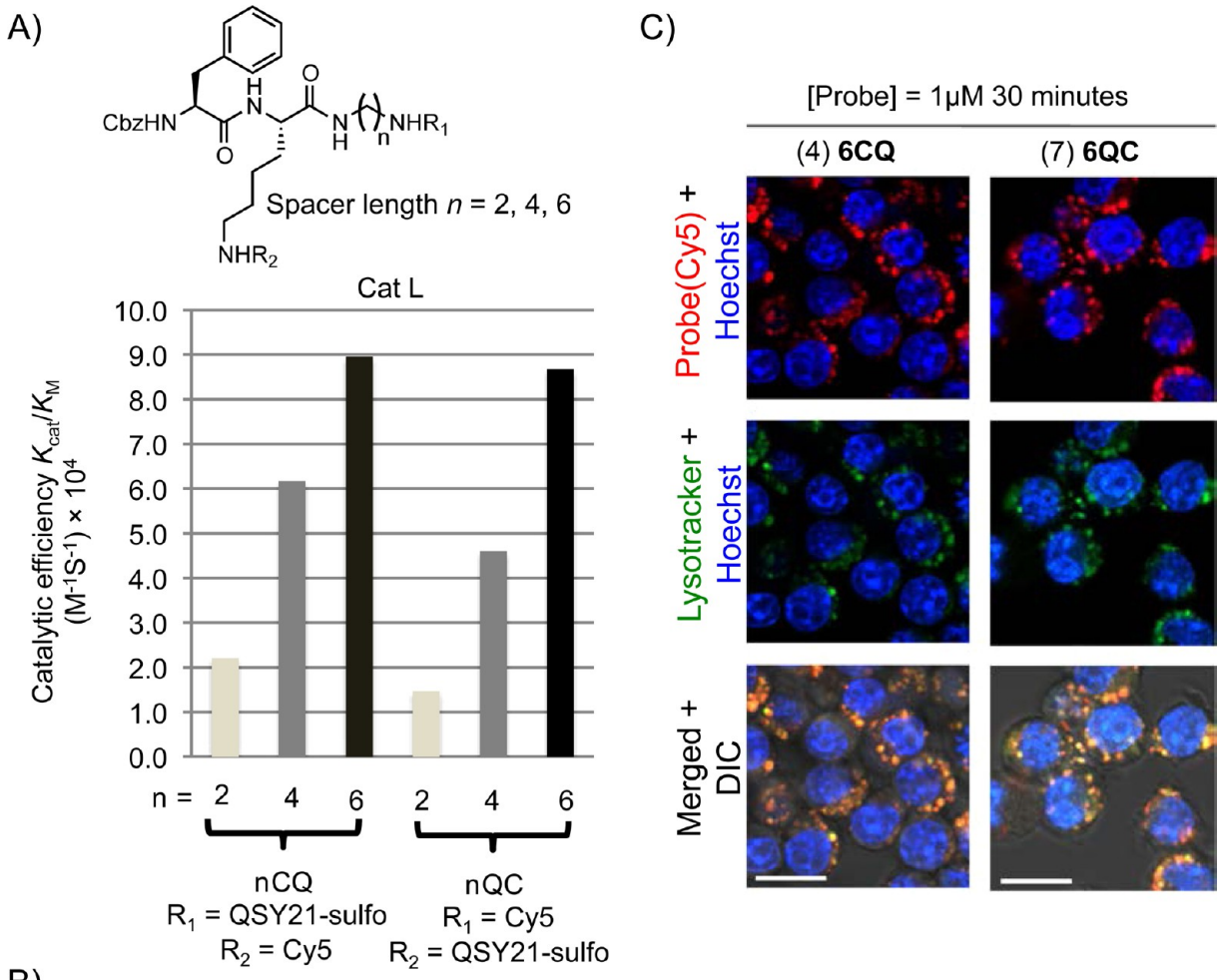

B)

probe	K_M (μM)	K_{cat}(s^{-1})	K_{cat}/K_M($M^{-1}s^{-1}$)
(2) **2CQ**	6.4 ± 0.8	0.141	22094
(3) **4CQ**	4.6 ± 0.7	0.283	61744
(4) **6CQ**	5.4 ± 0.5	0.487	89551
(5) **2QC**	6.5 ± 1.5	0.095	14687
(6) **4QC**	8.6 ± 1.3	0.396	46008
(7) **6QC**	5.3 ± 0.8	0.458	86763

Figure 2. *In vitro* properties of the cathepsin probes. (A) Effect of varying spacer length "*n*" on cleavage efficiency (K_{cat}/K_M) of quenched substrates *n*CQ and nQC by recombinant cathepsin L. (B) Table of kinetic parameters of the quenched substrates for recombinant cathepsin L. Data represents an average of three replicate experiments ± standard error of the mean. (C) Representative live cell fluorescence microscopy images of RAW 264.7 cells incubated with 1 μM of quenched substrates followed by washout. Red is cy5 fluorescence of probes, green is lysosome selective stain), and blue is Hoechst 33342 (nuclear stain). Scale bar represents 10 μm.

response.[21] In general, cysteine cathepsin activities are elevated in virtually all solid tumors due to increased infiltration of immune cells.[22−25] The cysteine cathepsins have therefore been the target of several tumor-specific imaging agents. These include covalently binding quenched fluorescence activity-based probes (qABPs),[26−31] a range of high and low molecular weight quenched substrate probes,[32,33] and fluorogenic turn-on substrate probes.[34−36] Although all of the reported protease-triggered smart probes have proven useful for imaging of tumor margins in mouse models of cancer,[28,30,31,33,37,38] all have limitations in terms of overall signal brightness or tumor contrast and none have been used with clinically approved

DOI: 10.1021/acschembio.5b00205
ACS Chem. Biol. 2015, 10, 1977−1988

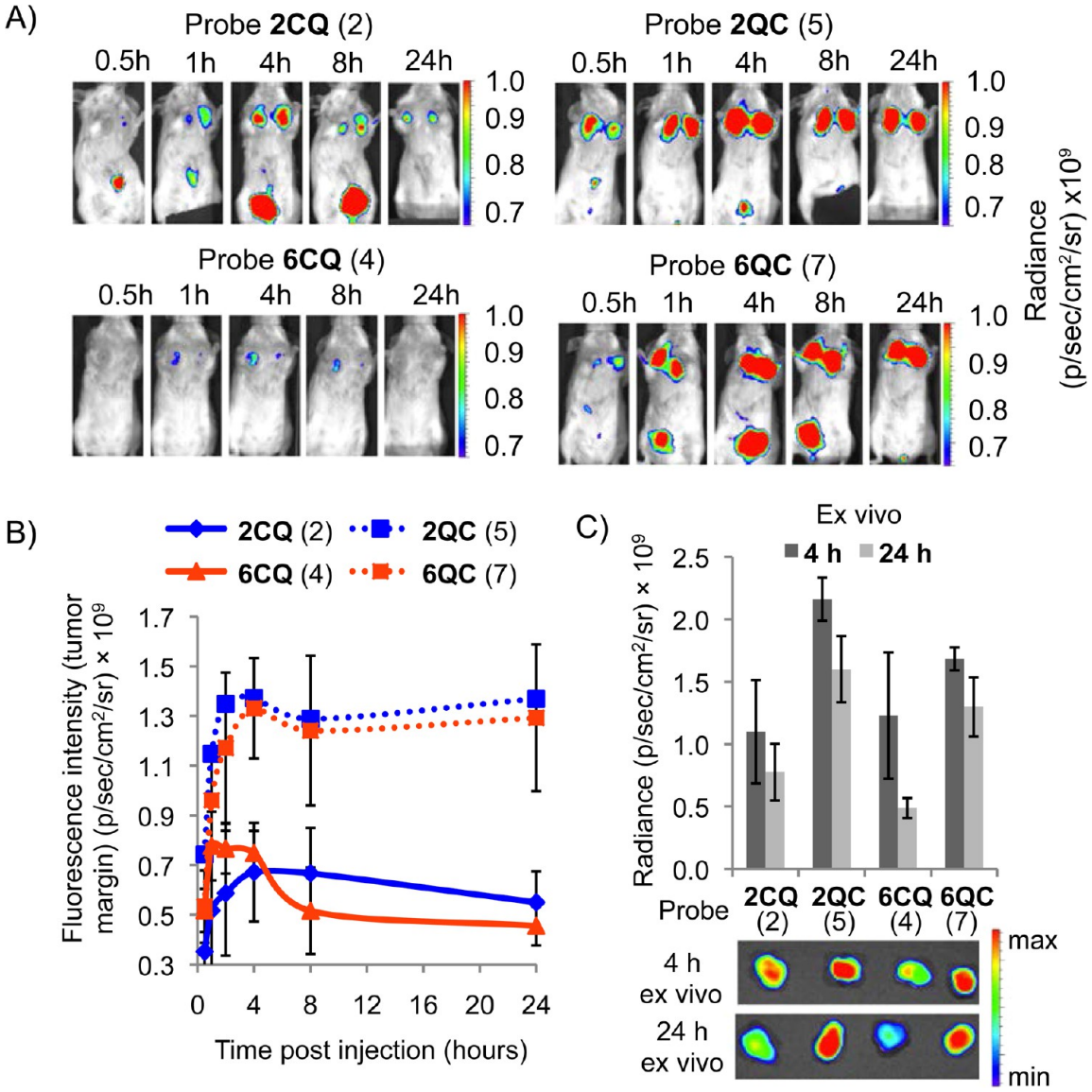

Figure 3. *In vivo* properties of the cathepsin substrate probes. (A) Time course of noninvasive fluorescence imaging of tumor-associated cysteine cathepsins in mice injected with substrates ***n*CQ/QC** (n = 2, 6). Representative images are shown for 0.5, 1, 4, 8, and 24 h time points. (B) Comparison of tumor-labeling kinetics of the nonlysosomotropic probes ***n*CQ** and the lysosomotropic ***n*QC** substrates over a period of 24 h. (Error bars represent the standard deviation on the mean of $N \geq 3$ mice. A control mouse without probe was used to correct for autofluorescence). (C) *Ex vivo* images of tumors at 4 h and at 24 h post injection of the two types of substrates. Error represent the standard deviation of the mean for $N \geq 3$ mice.

imaging instrumentation. Therefore, the optimization of a targeted contrast agent with enhanced contrast for multiple tumor types and that could be used with existing clinical instrumentation within the confines of existing surgical workflows would be transformative to many surgical procedures.

In this study, we report the design and optimization of a cathepsin-targeted fluorescence contrast agent that exploits a latent lysosomotropic effect (LLE) to achieve increased signal strength and durability in solid tumors by inducing probe accumulation in lysosomal compartments upon cleavage. We find that it is possible to enhance turnover of the substrate to increase imaging signals by optimizing the linker in the probe scaffold. The combination of optimized substrate scaffold and addition of the LLE results in probes suitable for clinical translation with high signal-to-noise ratios and extended retention in tumor tissues. Perhaps most importantly, we show that the optimized LLE substrate probes provide sufficient signal and contrast that they can be used in existing surgical workflows for real-time imaging of multiple solid tumor types using the da Vinci Surgical System (Intuitive Surgical, Sunnyvale, CA; www.intuitivesurgical.com/products/davinci_surgical_system/) that is currently in use in hospitals worldwide.

RESULTS

Design of Cathepsin Targeted Optical Contrast Agents. As a starting point of probe design, we used the primary scaffold of our recently reported[28] potent and selective qABP (Figure 1a, compound **1**) as a template. We hypothesized that the ability of the substrates to produce signal without inhibiting the target protease, coupled with an

DOI: 10.1021/acschembio.5b00205
ACS Chem. Biol. 2015, 10, 1977−1988

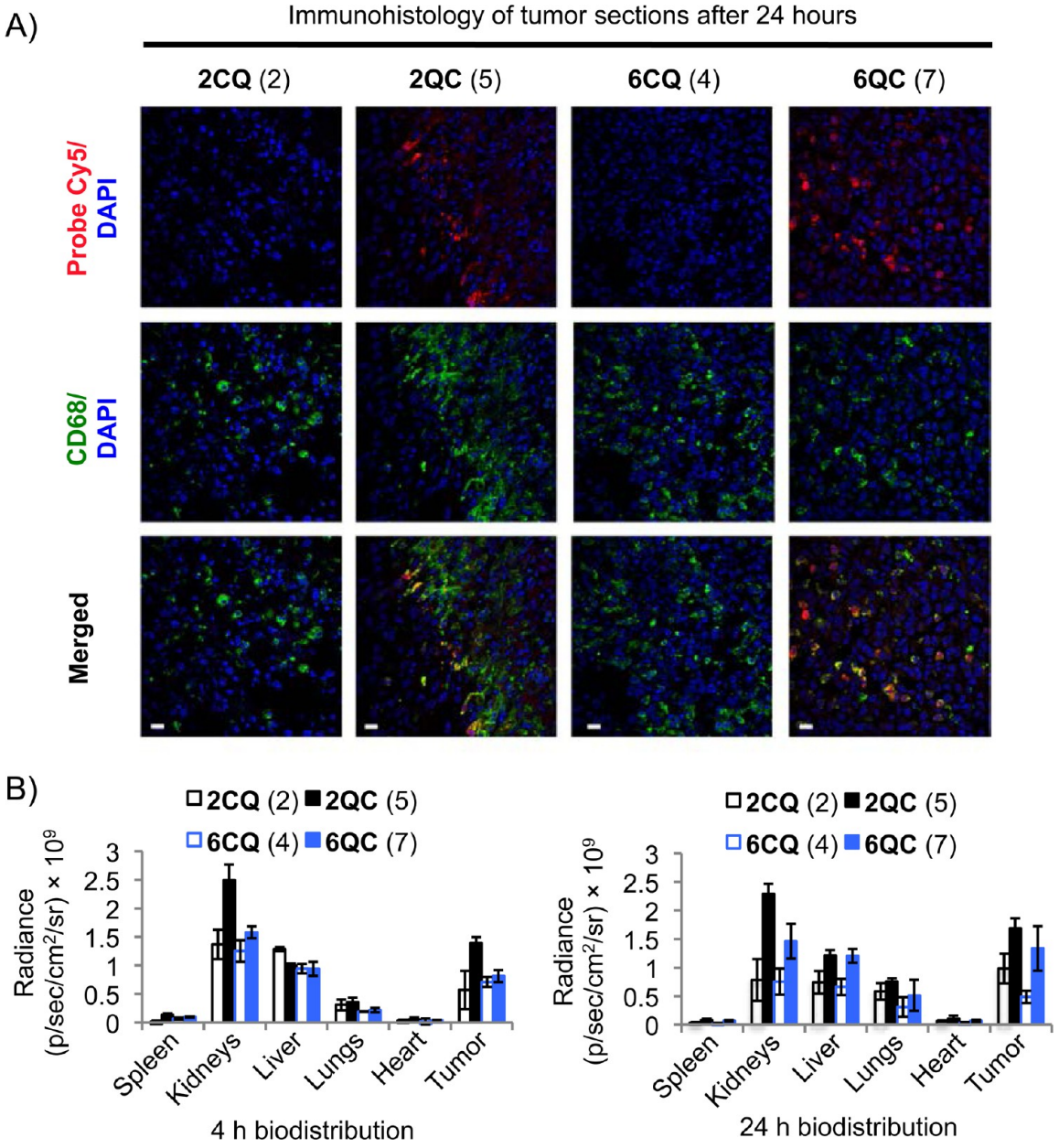

Figure 4. Analysis of cellular localization of activated substrates in tumor tissues (A) Immunohistology of frozen sections of tumors excised from mice injected with substrates ***n*CQ** and ***n*QC** at the 24 h time point. Red is the Cy5 fluorescence of probes, green is CD68 (macrophage marker), and blue is DAPI (nuclear stain). Scale bar represents 10 μm. (B) Biodistribution of probes in various organs after 4 and 24 h following intravenous administration of the indicated probes. Errors represent the standard deviation of the mean for $N \geq 3$ for each time point.

improved aqueous solubility, would create substrate analogues that activate faster and produce brighter signal *in vivo* compared to the original covalent probes. We installed a cleavable amide bond in place of the irreversible thiol-reactive tetrafluorophenoxymethyl ketone (PMK) electrophile and then examined the effect of varying the length of the alkyl spacer between the cleavage site and the quenching group on enzyme turnover. We initially chose three different spacer lengths, ranging from n = 2, 4 and 6, methylene groups, representing probes **2CQ** (2), **4CQ** (3) and **6CQ** (4), where the letters C and Q represents the chromophore and quencher, respectively, and the number indicates the spacer length.

In addition to considering the dynamics of enzyme turnover, one of the major limitations of substrate-based probes is the rapid diffusion of the fluorescent fragments after cleavage by the protease. Several approaches have been developed to increase the signal of noncovalent imaging agents in tumors. However, all have involved the attachment of additional moieties (e.g., PEG, lipids, etc.) to alter the properties of the intact probe, which can lead to increased background and slower tumor uptake.[33,39] We reasoned that it should be possible to exploit a latent lysosomotropic effect (LLE) in which a substrate is cleaved to produce a fluorescent fragment that accumulates in lysosomes due to protonation of the free amine that is produced by the proteolytic event.[40] Protonation of this fragment in lysosomes (pH ∼4−5) reduces the diffusion rate of the cationic charged intermediate across the lysosomal membrane.[41] This buildup of the trapped fluorophore-containing fragment should result in an increase in the strength, stability, and overall durability of the signal in tumors.

DOI: 10.1021/acschembio.5b00205
ACS Chem. Biol. 2015, 10, 1977−1988

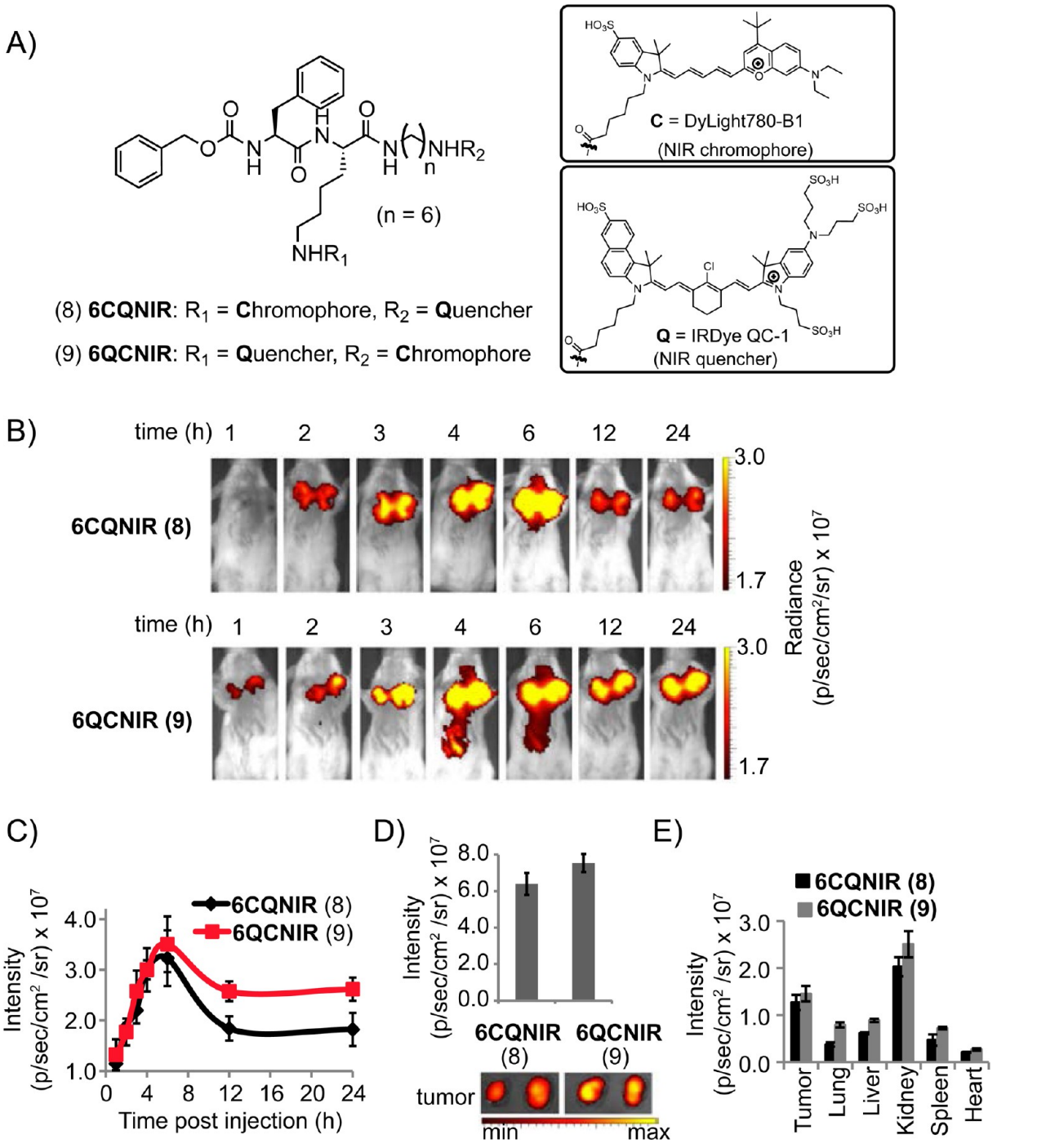

Figure 5. Evaluation of *in vivo* properties of optimized NIR probes. (A) Chemical structures of the near-infrared quenched lysosomotropic substrate **6CQNIR** (8) and nonlysosomotropic analogue **6QCNIR** (9). (B) Time course of noninvasive fluorescence imaging of tumor associated cysteine cathepsins in the 4T1 breast cancer mouse model using the NIR probes. (C) Quantification of tumor-labeling kinetics of 6CQNIR and 6QCNIR over the 24-h time course. $N \geq 3$ mice for each probe. Error bars represent the standard deviation on the mean. (D) *Ex vivo* images comparing tumors isolated from mice that received the LLE (9) and non-LLE (8) substrates at the 24 h time point. (E) Biodistribution of probes in various organs and tumors 24 h after injection.

Thus, to take advantage of the LLE, we interchanged the location of the chromophore (C) and quencher (Q) to generate probes **2QC** (5), **4QC** (6) and **6QC** (7), which produce free amine-containing fluorescent products upon proteolysis (Figure 1b). Importantly, this design approach does not change the core structure or size of the probe and the lysosome trapping effects is only exposed after the cathepsin has activated the internalized probe in lysosomes.

We synthesized all six substrate probes in good yields using a combination of solid- and solution-phase chemistries (see Supporting Information Scheme S1). The initial substrates contained the Cy5 chromophore and sulfo-QSY21 as the quencher. We first tested the probes for activity *in vitro* by monitoring the product curves of each internally quenched probe in the presence of recombinant cysteine cathepsin L, S, K, B, and V. All of the quenched substrates (*n*QC/*n*CQ, *n* = 2,

DOI: 10.1021/acschembio.5b00205
ACS Chem. Biol. 2015, 10, 1977–1988

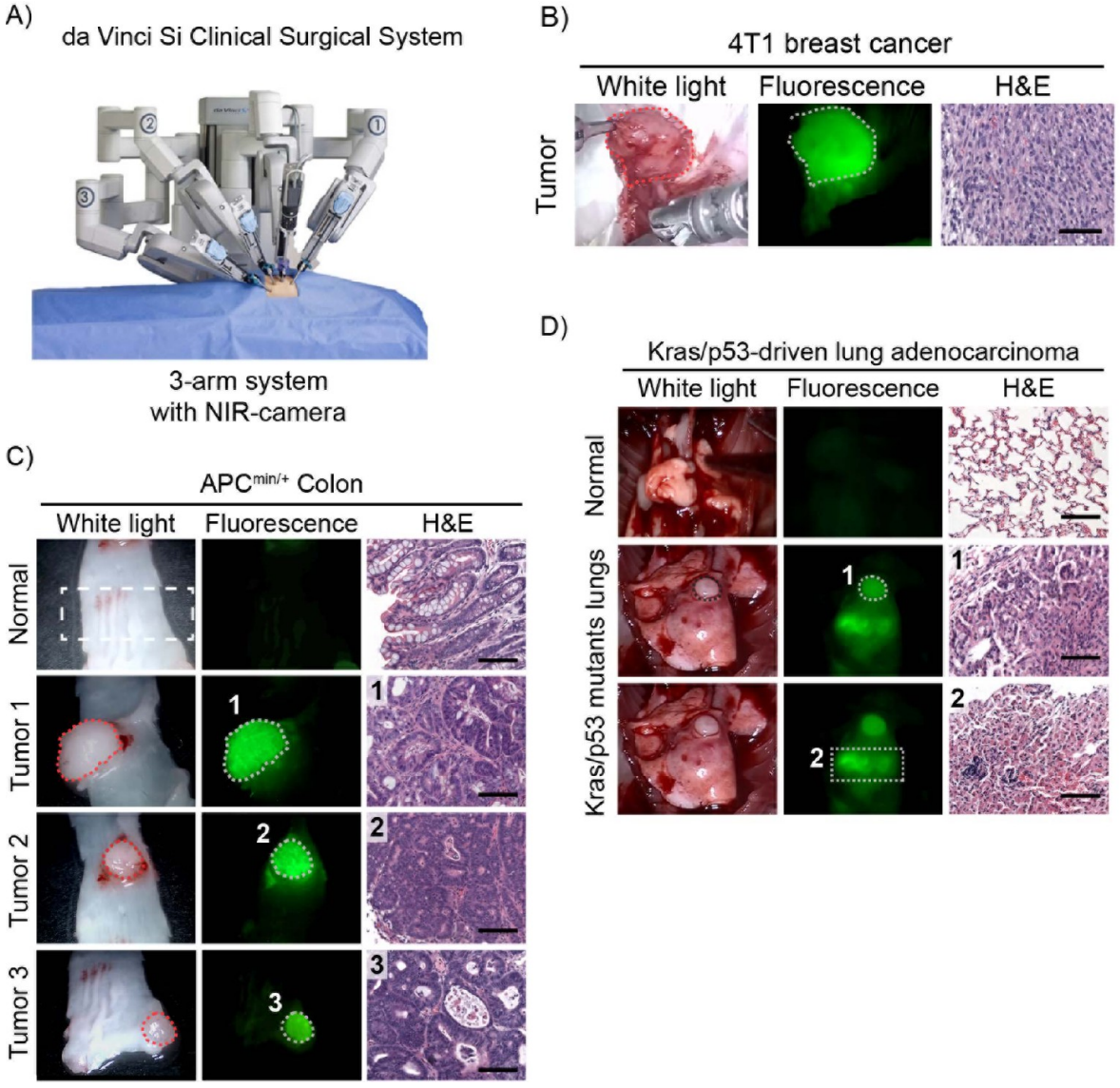

Figure 6. Intraoperative fluorescence image guided detection and resection of colorectal, breast, and lung tumors using the da Vinci Surgical System. (A) Image of the da Vinci Surgical System. (B) Detection and fluorescent image guided surgical removal of mouse breast tumors (4T1) using the da Vinci instrument 6 h after I.V. treatment with contrast agent 6QCNIR. The image is a screen capture from Movie S1 showing white light illumination of tumor and tumor bed (left), as well as corresponding fluorescence image detected using the Firefly camera system on the da Vinci instrument (center). Tissue histology of the resected region (dashed lines) as assessed by H&E stain is shown at right. (C) Detection of polyps in the colon of colorectal cancer APC^{min+} mouse model 6 h after I.V. administration of 6QCNIR. Images are screenshots from Movie S2. The panels show representative images of polyps detected by white light illumination of tumors (left) and subsequent fluorescence imaging using the Firefly camera (center). Tissue histology of the resected regions (dotted lines) as assessed by H&E stain is shown at right. The white dashed box shows a general region of normal tissue used for histology. (D) Images of mice bearing lung adenocarcinomas in the $Kras^{LSL\text{-}G12D/+}$; $p53^{flox/flox}$; $R26^{LSL\text{-}tdTomato/+}$ (KPT) mouse model 6 h after I.V. administration of the 6CQNIR probe. Images were take from Movie S3 as in B and C and tissues analyzed by H&E staining of tissue slices taken from the tissues in the regions shown (dashed lines). The white dashed box shows a general region showing increased fluorescence that was confirmed by histology to be cancerous. Scale bars for all H&E images are 100 μM.

4, 6) were cleaved by cathepsins L, V, S, and K (Supplementary Figure 1). Importantly, the cleavage of the substrates was not affected by the orientation of the chromophore and quencher pair on the substrate, with both *n*CQ and *n*QC probes being cleaved at similar rates (Figure S1). In contrast, there was a strong correlation between the catalytic/cleavage efficiency (K_{cat}/K_M) and the length of the alkyl spacer of the substrate, with all cathepsins more effectively processing the substrates with the longest $n = 6$ linker (Figure 2A). These differences in catalytic efficiencies resulted exclusively from differences in the catalytic rate constants (k_{cat}), as K_M values were virtually identical for all substrates (Figure 2b).

One hallmark of almost all forms of cancers is the increased infiltration of immune cells such as macrophages into the tumor as well as the surrounding margins.[20,42] Therefore, in order to validate the LLE hypothesis, we measured probe activation in a macrophage derived cell line RAW264.7. We observed strong probe fluorescence in cells incubated with each of the quenched substrates, suggesting that these probes are indeed activated by lysosomal cysteine proteases in this macrophage derived cell line (Figure 2c). Labeling in the live cells was selective to

DOI: 10.1021/acschembio.5b00205
ACS Chem. Biol. 2015, 10, 1977−1988

lysosomes as confirmed by the strong colocalization of the probe with the lysosome specific marker Lysotracker Red. The similar labeling intensity of the *n*CQ and *n*QC probes in live cells suggests that the probes are internalized at similar rates suggesting that the placement of the fluorophore does not perturb uptake of the probes.

Noninvasive Optical Imaging of Solid Tumors. We initially tested the probes in a syngeneic, orthotopic mouse model of breast cancer. In this model, 4T1 cells are inoculated into the number 1 and 10 mammary fat pad of mice to generate tumors. In order to determine the impact of the LLE, we directly compared imaging signals of lysosomotropic probes **2QC** (5) and **6QC** (7) to that of the nonlysosomotropic analogues **2CQ** (2) and **6CQ** (4). We intravenously administered probes to tumor-bearing mice and then performed noninvasive imaging at various time points post probe injection. We observed rapid accumulation of Cy5 fluorescence from activation of the probes in and around the tumors in less than 30 min with sufficient contrast demarcating tumor from the surrounding normal tissues within 1 h (Figure 3a). The intensity of the fluorescent signal reached a maximum at 4 h after administration, followed by retained high signals for 24 h (Figure 3b). Importantly, the overall absolute fluorescence intensity in the tumors was higher and brighter for mice treated with the LLE substrates 2QC and 6QC compared to the nonlysosomotropic analogs 2CQ and 6CQ. Furthermore, the intensity of the signal remained constant over a period of 24 h in the tumors of mice administered with the LLE substrates, whereas the signals from the non-LLE substrates substantially reduced after 24 h (Figure 3a, b). A similar trend was observed by *ex vivo* imaging of the excised tumors at 4 h and at the end of the 24 h period (Figure 3c).

In order to determine if the LLE probes demonstrate specific accumulation in tumor tissues relative to the non-LLE and definitively confirm this mechanism of accumulation, we performed fluorescence microscopy analysis on isolated tumor tissues from mice treated with the probes. This also allowed us to determine which populations of cells are responsible for activating the quenched substrate probes *in vivo*. Importantly, this immunofluorescence staining showed that the probe signal was found exclusively in CD68-positive cells (macrophages) and was only visible for the LLE probes (2QC and 6QC), when tissues were analyzed by histology 24 h post probe injection (Figure 4a). Further analysis of various organs from the 4 h and 24 h time points showed that most organs take up the probes. However, the strongest accumulation of the probe was observed in the kidneys and the tumor, suggesting that they are eliminated mainly by renal clearance (Figure 4b). Together, these results confirm that the LLE leads to enhanced probe retention in tumors as the result of lysosomal retention of the fluorescent products of the probe.

Application of Probes in FGS Using the da Vinci Surgical System. The da Vinci Surgical System[43] is one example of a clinically approved instrument for minimally invasive surgical procedures. Most da Vinci procedures are performed using white light illumination with no contrast to guide the surgeon in real time. We therefore set out to test our optimized substrate probes using the da Vinci system employing the same workflows that are used in the clinic. In order to achieve a real-time intraoperative imaging capability, we synthesized our probes containing a near-infrared (NIR) fluorophore DyLight780-B1 and corresponding QC-1 NIR quencher (**6CQNIR** (8) and **6QCNIR** (9)) so that they would be compatible with the existing camera of the da Vinci system (Figure 5a; Supplemental Scheme 2). Prior to application with the da Vinci system, we validated the probes in the 4T1 breast cancer model described above using the IVIS-spectrum small animal imaging system. Following systemic administration of the NIR cathepsin-targeted contrast agents, we imaged mice noninvasively every hour for 4 h, and then at 6, 8, 12, and 24 h. As observed for the Cy5 labeled probes, we observed a rapid accumulation of the probe signal in and around the breast tumors, with substantial contrast demarcating the tumor margin from healthy surrounding tissues as early as 1 h post injection (Figure 5b). The intensity of the fluorescence signal in the tumors increased rapidly in mice injected with both types of probes, which eventually peaked between 4 and 6 h. Similar to the initial Cy5 substrates, the NIR analogues showed the LLE as evidenced by the increased signals of the LLE probe in tumors in live animals (Figure 5b,c) and after *ex vivo* analysis of tumors (Figure 5d). Signal intensity was similar for both probes at the 1 and 4 h time points, suggesting equal rates of diffusion into tissues as well as similar activation rates. However, the LLE probes showed brighter signals and longer retention in tumors starting at 6 h after injection (Figure 5c). Interestingly, the LLE in the NIR substrates was a somewhat weaker effect relative to the Cy5 substrates, likely due to the extra cationic charge on the benzopyrillium ring on the Dylight 780-B1 dye (Figure 5a). This charge confers some degree of lysosomotropism to the uncleaved substrates and thus reducing the overall relative enhancement of retention as the result of cleavage by a protease. Similar to the Cy5 probes, these NIR analogues were eliminated by renal clearance as we observed highest signal accumulation in the kidneys and tumors (Figure 5e).

We next applied the probes directly in intraoperative fluorescence image guided surgery using the da Vinci system (Figure 6a). For these studies, we focused on the 6QCNIR probe because it had the brightest signal and the longest tumor retention. In order to demonstrate that the probe can be employed as a common targeted contrast reagent for FGS of diverse tumors, we performed validation studies in three mouse models of cancer. These studies included the 4T1 breast cancer transplant model as well as two spontaneous cancer models of lung and colon cancer (Kras/p53 driven lung cancer model[44] and APC^{min+} colorectal adenoma model[45]).

We initially performed the da Vinci surgery on mice containing 4T1 implanted breast tumors at 6 h after administration of the LLE probe (Supplementary Movie S1). Using real-time intraoperative fluorescence imaging, we were able to clearly detect strong probe signal in tumors relative to surrounding tissue (Figure 6b). After surgical removal of the primary tumor, the fluorescent contrast allowed detection of secondary tumors, buried deep in the tumor bed (Supplementary Movie S1, starting at 0:55). As expected, these secondary tumors could not be distinguished from the normal surrounding tissues under white light, but we could resect them intraoperatively when guided by the probe signal. Analyses of resected probe positive tissues (including the secondary tumors) by histology using hematoxylin and eosin (H&E) staining confirmed that they were all indeed cancerous tissues (Figure 6b).

As a second model to test the probes, we performed a direct FGS imaging study using the $APC^{min/+}$ model. This model is an ideal choice as it mimics human colon cancer with tumors forming spontaneously in the colon. For this model, we performed surgery using the da Vinci system to remove the

DOI: 10.1021/acschembio.5b00205
ACS Chem. Biol. 2015, 10, 1977−1988

colon. We then flushed, splayed open, and imaged the colon with the wide field camera of the da Vinci under both white light and NIR illumination (Supplementary Movie S2). In fluorescence mode, we were able to unambiguously identify, in real time, multiple intestinal polyps with various morphologies along the entire length of the colon. The probe labeled the malignant polyps with high signal intensity and with good contrast demarcating the tumor from the surrounding healthy colon. In addition to the intestinal adenomas, we observed some signal in the mucosal colonic patches, suggesting cathepsin activity. We removed the probe-positive polyps using intraoperative real-time fluorescence imaging to ensure complete resection of the tumors from the tumor beds (real-time video is shown in Movie S2). Subsequent analysis of the resected tumor tissues by H&E staining confirmed that all the probe positive polyps were indeed tumors (Figure 6c) with the exception of a few small foci that were found to be colonic patches. No signal increase above background was observed in the colon of control healthy mice administered with the same dose of the contrast agent, confirming that the activation of the probe is due to the high levels and activity of cathepsins in tumors.

As a final test of the overall broad applicability of the contrast agent, we performed imaging studies in a lung adenocarcinoma mouse model in the *Kras*$^{LSL\text{-}G12D/+}$; *p53*$^{flox/flox}$; *R26*$^{LSL\text{-}tdTomato/+}$ (KPT) mouse model of adenocarcinoma[46] in which lung tumors are induced in mice by intratracheal infection with lentiviral delivering Cre recombinase.[44] As performed for the other two models, we intravenously treated mice with the 6QCNIR probe 6 h prior to FGS. We opened the chest cavity prior to the surgery and were able to detect lung adenomas intraoperatively using real-time fluorescence imaging on the da Vinci system (Supplemental Movie S3). We were able to detect tumors in the lungs with high contrast differentiating tumor from normal lung tissues (Figure 6d). Furthermore, we observed small secondary regions of probe signal that were not visible by white light imaging. All of the probe positive tissues were removed from the lungs and confirmed to be tumor-derived by histology. Control mice injected with the same dose of the contrast agent showed only background fluorescence, consistent with low levels of cathepsin activity in the lung tissues.

DISCUSSION

Laparoscopic surgery, also known as minimally invasive surgery, is becoming popular for removing various solid tumors due to faster recovery time, reduced blood loss, pain, and rates of infection. The da Vinci Surgical System produced by Intuitive Surgical (Sunnyvale, CA) is one example of a clinically approved surgical system that is in use in hospitals around the world for robotic-assisted resection of various kinds of tumors.[47] Surgical resection is currently the most common form of treatment for most types of solid tumors. In order to improve treatment outcomes and minimize subsequent future recurrence, it is critical to remove all the cancerous tissues from the affected organ.[48] Targeted fluorescence contrast agents capable of distinguishing between cancerous and normal tissues have the potential to guide intraoperative, real-time decision-making and thereby improved the outcomes of surgical treatments. In spite of these advantages, there are currently no FDA approved molecular targeted optical contrast agents. Current resections of tumor are therefore performed without any additional contrast to demarcate the margins of tumors.

In this report, we have developed a cathepsin-targeted, tumor-selective substrate probe 6QCNIR (9) that is compatible with existing clinical instrumentation for use in fluorescence image guided surgery. In the process of optimizing the cathepsin targeted probes to improve *in vivo* pharmacokinetics and pharmacological properties, we exploited a latent lysosomotropic effect (LLE). This strategy allowed us to enhance the signal intensity and increase the signal to background ratio of the probes by trapping the released fluorophore in lysosomes once cleaved by a protease. The use of cleavable substrate probes in noninvasive imaging is often hindered by poor signal to background as the result of fast diffusion of the activated fluorophore from the tumor site to the surrounding tissues. In theory, quenched fluorogenic substrates should be advantageous due to signal amplification as the result of substrate turnover by the protease. However, rapid renal clearance of the products reduces signal at a rate that is fast enough to mitigate this advantage.[49,50] As a result, several approaches have been employed to stabilize the signal in the tumor milieu. Examples of such approaches include the conjugation of high molecular weight polyethylene glycol (PEG) linkers to the substrate to increase circulation and slow clearance,[39] and lipidation by conjugation of palmitate to increase membrane retention.[33] However, both of these approaches result in significant changes to the size and properties of the uncleaved probes, thus leading to reduced tumor uptake and higher background in normal tissues. Our strategy exploiting the LLE does not modify the substrate because it requires no introduction of additional structural components, and furthermore, the increased retention is only observed in the cleaved product.

In support of the value of the LLE probes for FGS, we found that the probes provided optimal contrast in diverse tumor types. In the 4T1 breast cancer model, rapid accumulation of the activated probe could be observed in the tumor with sufficient contrast to differentiate the tumor from normal surrounding tissues in less than 1 h after administration. The signal in the tumors of the group of mice that received the LLE probe persisted in the tumor area for more than 24 h. In addition, the overall absolute fluorescent intensity and contrast was higher compared to the non-LLE substrates. In the APC^{min+} colorectal cancer model, the cathepsin targeted probe was able to detect all adenomas present in the colon, including early lesions that were relatively flat, akin to those often difficult to detect using current endoscopic methods. H&E staining of the polyps showed that the probe detected adenomas with very high efficiency. This suggests that, when coupled with conventional methods of colonoscopy (which is currently carried out only under white light), the reported probes can enhance the detection of polyps at various stages and sizes, and hence improve the outcome of screening and treatment of colorectal cancer.

We believe that the cathepsin targeted probes presented here can be broadly used to image solid tumors of diverse origins, due to the fact that cathepins are overexpressed in virtually all cancer types. Furthermore, because increased cathepsin activity is associated with inflammation in conditions such as atherosclerosis, asthma, stroke, and sepsis, these probes have the potential to be used for detection and treatment of many other conditions. Most importantly, our data suggest that this probe can be used as a targeted contrast agent in FGS in conjunction with an FDA approved clinical instrument that is currently in use in hospitals worldwide.

DOI: 10.1021/acschembio.5b00205
ACS Chem. Biol. 2015, 10, 1977−1988

MATERIALS AND METHODS

Compound Synthesis. All reagents and materials used in the synthesis of the noncovalent fluorescently quenched cysteine cathepsin targeted contrast agents were obtained from commercial sources and were used without additional purification. Cy5-NHS ester and QSY21-sulfo-NHS ester were synthesized using reported procedures. DyLight 780-B1-NHS ester was obtained from Pierce (Thermo Scientific, Cat. No. 53064), and IRDye QC-1 NHS ester (near-infrared quencher) was purchased from LI-COR Bioscience (Lincoln, Nebraska). Compounds were synthesized by a combination of solid and solution phase synthesis, followed by purification of the final products by reverse phase preparative HPLC. Detailed synthetic procedures including compound characterization are given in the Supporting Information.

In Vitro Enzyme Kinetics with Quenched Substrates. Recombinant cysteine cathepsins (including Cat. L, B, S, V, and K) were obtained commercially. The concentration of the enzymes used in the kinetic assay were first confirmed by active site titration using the irreversible inhibitor ZFK-Chloromethyl ketone and the commercial substrates Z-VVR-AMC for cathepsns, S, L, B, and V, or Z-KR-AMC for cathepsin K. Initial screening of the synthesized substrate for activity against the different cathepsins was performed by the incubation of a fixed concentration of each probe with the protease dissolve in 50 mM citrate buffer (pH = 5.5, 5 mM DTT, 0.1% triton X, 0.5% CHAPS) at 37 °C in a black opaque 96-well plate. Turnover curves were followed by measuring the increase in Cy5 fluorescence (640/670 nm) using a Biotek plated reader. For the measurement of kinetic parameters, an equal concentration of each enzyme (final concentrations of 5 nM) was incubated with each of the different types of quenched substrate. The rates of increase in Cy5 fluorescence (which is indicative of probe cleavage by cathepsins) were measured for each concentration (a serial dilution starting from a final concentration of 10 μM to 0 μM in triplicate) of quenched substrate from the linear portion of the turnover curves. The kinetic parameters (K_m, K_{cat} and K_m/K_{cat}) were obtained by fitting the experimental data to the Michaelis Menten equation using GraphPad Prism software.

Live Cell Imaging. RAW246.7 cells were seeded in a 35 × 10 mm glass bottom tissue culture dish at a density of approximately 1×10^4 cells 24 h prior to labeling. The medium (Dulbecco's Modified Eagle's medium, DMEM supplemented with 10% fetal bovine serum, and 100 units/ml % penicillin and 100 μg/mL streptomycin) was replaced with 1 mL DMEM containing 1 μM of the indicated quenhced probe and incubated for 30 min in a humidified at 37 °C with 5% CO_2 atmosphere. After washing (1×) with PBS, the cells were incubated with fresh media containing 60 nM Lysotracker for 30 min followed by another wash with PBS. Subsequently, 5 μg/mL of Hoechst 33342 in DMEM was added and incubated for an additional 10 min. The cells were then washed (3×) with PBS and then covered with a layer of PBS for microscopy. Images were aquired using a 60× objective on Zeiss Axiovert 200 M confocal microscope using the filters for Cy5, Hoechst, and Lysotracker Red. Images were processed using ImageJ.

Animal Models. All animal care and experimentation was conducted in accordance with current National Institutes of Health and Stanford University Institutional Animal Care and Use Committee guidelines.

Breast Cancer. 4T1 cells were implanted into the mammary fat pad of 6−8 weeks old female BALB/c mice (The Jackson Laboratory, Bar Harbor, ME). Twenty-four hours before implantation, the hair on the region of interest was removed using "Nair lotion". A total volume of 100 μL of 1×10^6 4T1 cells (ATCC) in PBS was injected into mammary fat pad number 1 and 10 while the mice were under isoflurane anesthesia. Tumor growths were monitored for approximately 14 days. Twenty nanomolar (200 uM) of the indicated compound dissolved in a solution containing 20% or 10% DMSO in PBS was administered via tail vein. After injection, mice were imaged noninvasively at the indicated time points using either the IVIS 100 or IVIS-Spectrum systems (Xenogen). For the Cy5-containing compounds, the signal was detected with a Cy5.5 filter set, whereas the near-infrared dye was detected using 710 and 820 nm excitation and emission filters, respectively. Analyses of the images collected were performed with the Living Image software (PerkinElmer). After the last time point, the mice were anesthetized with isofluorane and sacrificed by cervical dislocation. Tumors and various organs were isolated by dissection and imaged ex vivo to measure the biodistribution profiles of the probes.

Colorectal Cancer. $APC^{min/+}$ on the C57BL/6 background were originally obtained from Jackson and maintained in a specific pathogen-free facility.

Lung Adenocarcinoma Mouse. The generation and intratracheal infection of $Kras^{LSL\text{-}G12D/+}$; $p53^{flox/flox}$; $R26^{LSL\text{-}tdTomato/+}$ (KPT) mice were as previously described in.[44,46] Briefly, 6 week old KPT mice were intratracheally infected with 4×10^3 Lenti-Cre virus and imaged/sacrificed 8 months postinfection. Noninfected age and sex-matched mice were used as controls.

Histology and Immunofluorescence. The resected tumors and control tissues were incubated in a 4% PFA solution in PBS for 6 h followed by an overnight incubation in a 30% sucrose solution. The fixed tissues were embedded and then frozen in OCT medium. Five micromolar sections were obtained on a glass slide and then fixed in acetone, blocked with PNB blocking buffer and incubated overnight with the macrophage marker rat antimouse CD68 (1:1000 AbD serotec Cat. No. MCA1957). Next, the tissues were incubated with the secondary antibody goat-anti rat conjugated with AlexaFluor-488 (1:500; Invitrogen) for 1 h at RT. Sections were then stained with DAPI (2 μg/mL; Invitrogen) for 5 min and then mounted in ProLong Gold Mounting Medium (Invitrogen). The sections were imaged at 40× using a Zeiss Axiovert 200 M confocal microscope in Cy5, FITC and DAPI channels. Isolated tumor tissues were fixed in 4% paraformaldehyde and then embedded in paraffin for sectioning. H&E staining was performed on the sectioned tissues as reported in the literature.

Intraopereative Fluorescence Guided Surgery with the da Vinci Surgical System. *Breast Tumors (4T1).* Tumor-bearing and control mice were administered the indicated probe intravenously (20 nmol in a solution of PBS with 10% DMSO) 6 h prior to surgery. A few minutes before surgery, mice were anaesthetized and euthanized by cervical dislocation and then mounted onto the surgical table. Surgery was performed using the da Vinci Surgical which is equipped with a CCD camera with near-infrared fluorescence imaging capability. Breast tumors were detected by fluorescence illumination and the solid tumors were removed using a combination of white and fluorescence light as a guide to confirm complete tumor resection. After removal of primary

DOI: 10.1021/acschembio.5b00205
ACS Chem. Biol. 2015, 10, 1977−1988

tumor the tumor bed was illuminated by near-infrared fluorescence to detect and remove residual or secondary malignant tissue. Real-time videos of the surgical procedures are shown in supplementary results (Movie S1). The tumors identified by the probe fluorescence were removed for further analyses by histology in order to confirm malignancy.

Colorectal Tumors. Apc mice were placed on a low fluorescence chow 72 h prior to surgery and then fasted for 12 h before surgery. 100 μL of 20 nmol of the indicated probe in PBS containing 10% DMSO was intravenously administered 6 h prior to surgery. Mice were then euthanized while under isoflurane anesthesia and then mounted onto the surgical table for FGS. The whole colon was observed for the presence of tumors using fluorescence. The colon portion of the intestine was then completely removed from the mouse, flushed with PBS to remove fecal matter, and then splayed open. Colonic polyps identified by fluorescence illumination of the splayed colon were subjected to histological analyses for positive confirmation of adenoma. Real-time videos of the surgical procedure of the FGS using the da Vinci system are shown in the supplementary results (Movie S2).

Lung Tumors. Tumor and control mice were administered intravenously with the indicated probe (20 nmol dissolved in PBS with 10% DMSO) 6 h before surgery. Mice were then euthanized while under isoflurane anesthesia and subsequently placed on the surgical table. The lung cavity was opened using the microforcep and scissor tools of the da Vinci system. Fluorescence illumination was used to detect the tumor margins and secondary tumors, which were excised and analyzed by histology for positive confirmation of malignancy. Real-time videos of the FGS procedures are shown in the supplementary results (Movie S3).

■ ASSOCIATED CONTENT

Supporting Information

The Supporting Information is available free of charge on the ACS Publications website at DOI: 10.1021/acschembio.5b00205.

■ AUTHOR INFORMATION

Corresponding Author

*E-mail: mbogyo@stanford.edu.

Present Address

[¶]Department of Tumor Immunology, Radboud Institute for Molecular Life Sciences, Radboud UMC Nijmegen, The Netherlands.

Notes

The authors declare no competing financial interest.

■ ACKNOWLEDGMENTS

This work was supported by NIH grants R01 EB005011 and R01 HL116307 (to M.B.) and an NIH Biomedical Sciences Supplement on R01 HL116307 (to L.O.O). We thank the members of the Bogyo laboratory for insightful discussions, T. Doyle at the Stanford Small Animal Facility, S. Lynch at the Stanford NMR Facility, and A. Chien and T. McLaughlin at the Stanford Mass Spectrometry Facility for their technical assistance.

■ REFERENCES

(1) Siegel, R., DeSantis, C., Virgo, K., Stein, K., Mariotto, A., Smith, T., Cooper, D., Gansler, T., Lerro, C., Fedewa, S., Lin, C., Leach, C., Cannady, R. S., Cho, H., Scoppa, S., Hachey, M., Kirch, R., Jemal, A., and Ward, E. (2012) Cancer treatment and survivorship statistics, 2012. *CA: A Cancer Journal for Clinicians 62*, 220−241.

(2) DeSantis, C. E., Lin, C. C., Mariotto, A. B., Siegel, R. L., Stein, K. D., Kramer, J. L., Alteri, R., Robbins, A. S., and Jemal, A. (2014) Cancer treatment and survivorship statistics, 2014. *CA: A Cancer Journal for Clinicians 64*, 252−271.

(3) Vahrmeijer, A. L., Hutteman, M., van der Vorst, J. R., van de Velde, C. J., and Frangioni, J. V. (2013) Image-guided cancer surgery using near-infrared fluorescence. *Nat. Rev. Clin. Oncol. 10*, 507−518.

(4) Miwa, S., Hiroshima, Y., Yano, S., Zhang, Y., Matsumoto, Y., Uehara, F., Yamamoto, M., Kimura, H., Hayashi, K., Bouvet, M., Tsuchiya, H., and Hoffman, R. M. (2014) Fluorescence-guided surgery improves outcome in an orthotopic osteosarcoma nude-mouse model. *J. Orthop. Res. 32*, 1596−1601.

(5) Fujita, T. (2012) Reality or dream of fluorescence-guided pancreatic cancer surgery? *J. Am. Coll. Surg. 215*, 591 author reply 592−593..

(6) Rudin, M., and Weissleder, R. (2003) Molecular imaging in drug discovery and development. *Nat. Rev. Drug Discovery 2*, 123−131.

(7) Bednar, B., Zhang, G. J., Williams, D. L., Jr., Hargreaves, R., and Sur, C. (2007) Optical molecular imaging in drug discovery and clinical development. *Expert Opin. Drug Discovery 2*, 65−85.

(8) Schaafsma, B. E., Mieog, J. S., Hutteman, M., van der Vorst, J. R., Kuppen, P. J., Lowik, C. W., Frangioni, J. V., van de Velde, C. J., and Vahrmeijer, A. L. (2011) The clinical use of indocyanine green as a near-infrared fluorescent contrast agent for image-guided oncologic surgery. *J. Surg. Oncol. 104*, 323−332.

(9) Tanaka, E., Choi, H. S., Fujii, H., Bawendi, M. G., and Frangioni, J. V. (2006) Image-guided oncologic surgery using invisible light: completed pre-clinical development for sentinel lymph node mapping. *Ann. Surg. Oncol. 13*, 1671−1681.

(10) Kovar, J. L., Simpson, M. A., Schutz-Geschwender, A., and Olive, D. M. (2007) A systematic approach to the development of fluorescent contrast agents for optical imaging of mouse cancer models. *Anal. Biochem. 367*, 1−12.

(11) van Dam, G. M., Themelis, G., Crane, L. M., Harlaar, N. J., Pleijhuis, R. G., Kelder, W., Sarantopoulos, A., de Jong, J. S., Arts, H. J., van der Zee, A. G., Bart, J., Low, P. S., and Ntziachristos, V. (2011) Intraoperative tumor-specific fluorescence imaging in ovarian cancer by folate receptor-alpha targeting: first in-human results. *Nat. Med. 17*, 1315−1319.

(12) Veiseh, M., Gabikian, P., Bahrami, S. B., Veiseh, O., Zhang, M., Hackman, R. C., Ravanpay, A. C., Stroud, M. R., Kusuma, Y., Hansen, S. J., Kwok, D., Munoz, N. M., Sze, R. W., Grady, W. M., Greenberg, N. M., Ellenbogen, R. G., and Olson, J. M. (2007) Tumor paint: a chlorotoxin:Cy5.5 bioconjugate for intraoperative visualization of cancer foci. *Cancer Res. 67*, 6882−6888.

(13) Turk, B. (2006) Targeting proteases: successes, failures and future prospects. *Nat. Rev. Drug Discovery 5*, 785−799.

(14) Drag, M., and Salvesen, G. S. (2010) Emerging principles in protease-based drug discovery. *Nat. Rev. Drug Discovery 9*, 690−701.

(15) McIntyre, J. O., and Matrisian, L. M. (2009) Optical proteolytic beacons for in vivo detection of matrix metalloproteinase activity. *Methods Mol. Biol. 539*, 155−174.

(16) Scherer, R. L., VanSaun, M. N., McIntyre, J. O., and Matrisian, L. M. (2008) Optical imaging of matrix metalloproteinase-7 activity in vivo using a proteolytic nanobeacon. *Mol. Imaging 7*, 118−131.

(17) Bremer, C., Tung, C. H., and Weissleder, R. (2001) In vivo molecular target assessment of matrix metalloproteinase inhibition. *Nat. Med. 7*, 743−748.

(18) Jiang, T., Olson, E. S., Nguyen, Q. T., Roy, M., Jennings, P. A., and Tsien, R. Y. (2004) Tumor imaging by means of proteolytic activation of cell-penetrating peptides. *Proc. Natl. Acad. Sci. U.S.A. 101*, 17867−17872.

(19) Nguyen, Q. T., Olson, E. S., Aguilera, T. A., Jiang, T., Scadeng, M., Ellies, L. G., and Tsien, R. Y. (2010) Surgery with molecular fluorescence imaging using activatable cell-penetrating peptides

DOI: 10.1021/acschembio.5b00205
ACS Chem. Biol. 2015, 10, 1977−1988

decreases residual cancer and improves survival. *Proc. Natl. Acad. Sci. U.S.A. 107*, 4317−4322.
(20) Shree, T., Olson, O. C., Elie, B. T., Kester, J. C., Garfall, A. L., Simpson, K., Bell-McGuinn, K. M., Zabor, E. C., Brogi, E., and Joyce, J. A. (2011) Macrophages and cathepsin proteases blunt chemotherapeutic response in breast cancer. *Genes Dev. 25*, 2465−2479.
(21) Mohamed, M. M., and Sloane, B. F. (2006) Cysteine cathepsins: multifunctional enzymes in cancer. *Nat. Rev. Cancer 6*, 764−775.
(22) Mitchem, J. B., Brennan, D. J., Knolhoff, B. L., Belt, B. A., Zhu, Y., Sanford, D. E., Belaygorod, L., Carpenter, D., Collins, L., Piwnica-Worms, D., Hewitt, S., Udupi, G. M., Gallagher, W. M., Wegner, C., West, B. L., Wang-Gillam, A., Goedegebuure, P., Linehan, D. C., and DeNardo, D. G. (2013) Targeting tumor-infiltrating macrophages decreases tumor-initiating cells, relieves immunosuppression, and improves chemotherapeutic responses. *Cancer Res. 73*, 1128−1141.
(23) McIntyre, J. O., and Matrisian, L. M. (2003) Molecular imaging of proteolytic activity in cancer. *J. Cell. Biochem. 90*, 1087−1097.
(24) Fonovic, M., and Bogyo, M. (2007) Activity based probes for proteases: applications to biomarker discovery, molecular imaging and drug screening. *Curr. Pharm. Des 13*, 253−261.
(25) Gocheva, V., Wang, H. W., Gadea, B. B., Shree, T., Hunter, K. E., Garfall, A. L., Berman, T., and Joyce, J. A. (2010) IL-4 induces cathepsin protease activity in tumor-associated macrophages to promote cancer growth and invasion. *Genes Dev. 24*, 241−255.
(26) Lee, J., and Bogyo, M. (2010) Development of near-infrared fluorophore (NIRF)-labeled activity-based probes for in vivo imaging of legumain. *ACS Chem. Biol. 5*, 233−243.
(27) Blum, G., Mullins, S. R., Keren, K., Fonovic, M., Jedeszko, C., Rice, M. J., Sloane, B. F., and Bogyo, M. (2005) Dynamic imaging of protease activity with fluorescently quenched activity-based probes. *Nat. Chem. Biol. 1*, 203−209.
(28) Verdoes, M., Oresic Bender, K., Segal, E., van der Linden, W. A., Syed, S., Withana, N. P., Sanman, L. E., and Bogyo, M. (2013) Improved quenched fluorescent probe for imaging of cysteine cathepsin activity. *J. Am. Chem. Soc. 135*, 14726−14730.
(29) Deu, E., Verdoes, M., and Bogyo, M. (2012) New approaches for dissecting protease functions to improve probe development and drug discovery. *Nat. Struct Mol. Biol. 19*, 9−16.
(30) Blum, G., von Degenfeld, G., Merchant, M. J., Blau, H. M., and Bogyo, M. (2007) Noninvasive optical imaging of cysteine protease activity using fluorescently quenched activity-based probes. *Nat. Chem. Biol. 3*, 668−677.
(31) Segal, E., Prestwood, T. R., van der Linden, W. A., Carmi, Y., Bhattacharya, N., Withana, N., Verdoes, M., Habtezion, A., Engleman, E. G., and Bogyo, M. (2015) Detection of Intestinal Cancer by Local, Topical Application of a Quenched Fluorescence Probe for Cysteine Cathepsins. *Chem. Biol. 22*, 148−158.
(32) Watzke, A., Kosec, G., Kindermann, M., Jeske, V., Nestler, H. P., Turk, V., Turk, B., and Wendt, K. U. (2008) Selective activity-based probes for cysteine cathepsins. *Angew. Chem., Int. Ed. 47*, 406−409.
(33) Hu, H. Y., Vats, D., Vizovisek, M., Kramer, L., Germanier, C., Wendt, K. U., Rudin, M., Turk, B., Plettenburg, O., and Schultz, C. (2014) In vivo imaging of mouse tumors by a lipidated cathepsin S substrate. *Angew. Chem., Int. Ed. 53*, 7669−7673.
(34) Kisin-Finfer, E., Ferber, S., Blau, R., Satchi-Fainaro, R., and Shabat, D. (2014) Synthesis and evaluation of new NIR-fluorescent probes for cathepsin B: ICT versus FRET as a turn-ON mode-of-action. *Bioorg. Med. Chem. Lett. 24*, 2453−2458.
(35) Chowdhury, M. A., Moya, I. A., Bhilocha, S., McMillan, C. C., Vigliarolo, B. G., Zehbe, I., and Phenix, C. P. (2014) Prodrug-inspired probes selective to cathepsin B over other cysteine cathepsins. *J. Med. Chem. 57*, 6092−6104.
(36) Fujii, T., Kamiya, M., and Urano, Y. (2014) In vivo imaging of intraperitoneally disseminated tumors in model mice by using activatable fluorescent small-molecular probes for activity of cathepsins. *Bioconjug Chem. 25*, 1838−1846.
(37) Mito, J. K., Ferrer, J. M., Brigman, B. E., Lee, C. L., Dodd, R. D., Eward, W. C., Marshall, L. F., Cuneo, K. C., Carter, J. E., Ramasunder, S., Kim, Y., Lee, W. D., Griffith, L. G., Bawendi, M. G., and Kirsch, D. G. (2012) Intraoperative detection and removal of microscopic residual sarcoma using wide-field imaging. *Cancer 118*, 5320−5330.
(38) Verdoes, M., Edgington, L. E., Scheeren, F. A., Leyva, M., Blum, G., Weiskopf, K., Bachmann, M. H., Ellman, J. A., and Bogyo, M. (2012) A nonpeptidic cathepsin S activity-based probe for noninvasive optical imaging of tumor-associated macrophages. *Chem. Biol. 19*, 619−628.
(39) Lee, D. W.; Bawendi, M. G.; Ferrer, J. Imaging Agent for Detection of Diseased Cells. U.S. Patent No. 20140301950, October 9, 2014.
(40) Kazmi, F., Hensley, T., Pope, C., Funk, R. S., Loewen, G. J., Buckley, D. B., and Parkinson, A. (2013) Lysosomal sequestration (trapping) of lipophilic amine (cationic amphiphilic) drugs in immortalized human hepatocytes (Fa2N-4 cells). *Drug Metab. Dispos. 41*, 897−905.
(41) Soulet, D., Gagnon, B., Rivest, S., Audette, M., and Poulin, R. (2004) A fluorescent probe of polyamine transport accumulates into intracellular acidic vesicles via a two-step mechanism. *J. Biol. Chem. 279*, 49355−49366.
(42) Bell-McGuinn, K. M., Garfall, A. L., Bogyo, M., Hanahan, D., and Joyce, J. A. (2007) Inhibition of cysteine cathepsin protease activity enhances chemotherapy regimens by decreasing tumor growth and invasiveness in a mouse model of multistage cancer. *Cancer Res. 67*, 7378−7385.
(43) Haber, G. P., White, M. A., Autorino, R., Escobar, P. F., Kroh, M. D., Chalikonda, S., Khanna, R., Forest, S., Yang, B., Altunrende, F., Stein, R. J., and Kaouk, J. H. (2010) Novel robotic da Vinci instruments for laparoendoscopic single-site surgery. *Urology 76*, 1279−1282.
(44) DuPage, M., Dooley, A. L., and Jacks, T. (2009) Conditional mouse lung cancer models using adenoviral or lentiviral delivery of Cre recombinase. *Nat. Protoc. 4*, 1064−1072.
(45) Moser, A. R., Pitot, H. C., and Dove, W. F. (1990) A dominant mutation that predisposes to multiple intestinal neoplasia in the mouse. *Science 247*, 322−324.
(46) Caswell, D. R., Chuang, C. H., Yang, D., Chiou, S. H., Cheemalavagu, S., Kim-Kiselak, C., Connolly, A., and Winslow, M. M. (2014) Obligate progression precedes lung adenocarcinoma dissemination. *Cancer Discovery 4*, 781−789.
(47) Mondal, S. B., Gao, S., Zhu, N., Liang, R., Gruev, V., and Achilefu, S. (2014) Real-time fluorescence image-guided oncologic surgery. *Adv. Cancer Res. 124*, 171−211.
(48) Hussain, T., Savariar, E. N., Diaz-Perez, J. A., Messer, K., Pu, M., Tsien, R. Y., Nguyen, Q. T. (2014) Surgical molecular navigation with a Ratiometric Activatable Cell Penetrating Peptide improves intraoperative identification and resection of small salivary gland cancers, *Head Neck* Dec 18. doi: 10.1002/hed.23946.
(49) Wittrup, K. D., Thurber, G. M., Schmidt, M. M., and Rhoden, J. J. (2012) Practical theoretic guidance for the design of tumor-targeting agents. *Methods Enzymol. 503*, 255−268.
(50) Thurber, G. M., Zajic, S. C., and Wittrup, K. D. (2007) Theoretic criteria for antibody penetration into solid tumors and micrometastases. *J. Nucl. Med. 48*, 995−999.

DOI: 10.1021/acschembio.5b00205
ACS Chem. Biol. 2015, 10, 1977−1988